RSC Advances

Energetic stability and photocatalytic activity of $SrTiO_3$ nanowires: *Ab initio* simulations

Journal:	*RSC Advances*
Manuscript ID:	RA-ART-01-2015-000306.R1
Article Type:	Paper
Date Submitted by the Author:	25-Feb-2015

Complete List of Authors:	Zhukovskii, Yuri; Institute of Solid State Physics, University of Latvia, Bandura, Andrei; St. Petersburg state university, Chemical Evarestov, Robert; St. Petersburg state university, Chemical

Energetic stability and photocatalytic activity of $SrTiO_3$ nanowires: *Ab initio* simulations

Andrei V. Bandura[1], Robert A. Evarestov[1] and Yuri F. Zhukovskii[2*]

[1]St. Petersburg State University, Quantum Chemistry Department, Petergof, St. Petersburg, Russian Federation
[2]Institute of Solid State Physics, University of Latvia, Riga, Latvia

Abstract. First principles periodic calculations based on the density functional theory within the localized atomic orbital approach (DFT-LCAO) using the hybrid exchange-correlation potential PBE0 have been performed in order to simulate the structural and electronic properties of both stoichiometric and non-stoichiometric [001]-oriented four-faceted $SrTiO_3$ (STO) nanowires (NW) of cubic structure. Their diameters have been varied from 0.3 up to 2.4 nm with a correspondence to a consequent change of NW cross-section from 2×2 to 5×5 extension of the lattice constant in bulk. Energetic stability of STO NW (both stoichiometric and non-stoichiometric) has been found to be increased with the decrease of their formation energies together with the increase of NW diameter. The electronic structure calculations have shown that the width of band gap is changed in STO NWs of different structural types as compared to that in bulk being consequently reduced with the growth of NW diameter although character of such a decrease depends on morphology of nanowire. Analysis of these changes shows that stoichiometric and non-stoichiometric TiO_2-terminated strontium titanate nanowires can be quite promising candidates for further applications in photocatalytic processes under solar irradiation whereas SrO-terminated NWs are rather not suitable for this purpose.

1. Introduction

Recent advances in science and technology of perovskites (ABO_3) and other ternary metal oxides ($A_xB_yO_z$) have resulted in the marked decrease of their sizes down to nanoscale dimensions which manifest essential deviation from the properties of 3D bulk and 2D film counterparts [1]. The two most widespread technological applications determine permanently growing interest to $A_xB_yO_z$ nanomaterials. Firstly, as a result of *ferroelectric* transition [2,3], the equilibrium crystalline structure of these materials is expected to be non-cubic, mainly tetragonal (*e.g.*, $BaTiO_3$, $PbTiO_3$) and trigonal (*e.g.*, $LiNbO_3$). On the other hand, ternary oxides are suitable for the *photocatalytic* water splitting into H_2 and O_2 gas components under solar irradiation [4,5]. Materials with perovskite cubic ($CaTiO_3$, $SrTiO_3$) and non-cubic, *e.g.*, orthorhombic ($NaNbO_3$, $KNbO_3$) as well as hexoctahedral ($Bi_2Ti_2O_7$), equilibrium structures are found to be fitted for such applications. As compared to other 0D and 1D nanoscale structures, ternary oxide nanowires (NWs) possess a higher efficiency in ferroelectric and photocatalytic applications. A unique feature of nanowires is that they are two-dimensional quantum confinement, while still leaving one unconfined direction for the transport of carriers [1,2,4], due to the uniformity along the chosen crystallographic axis, strong dependence of NW properties on intrinsic size effects and configuration of lateral facets.

A number of electrochemical and thermochemical methods were used for synthesis of single-crystalline $A_xB_yO_z$ (*e.g.*, $SrTiO_3$) nanowires [1,6-12]: (*i*) sol–gel or aqueous routes for fabrication of ordered NW arrays inside nanoporous silicon or alumina used as templates, (*ii*) solution-phase decomposition of bimetallic precursor in presence of coordinating ligands, (*iii*) molten-salt technique, (*iv*) hydrothermal or solvothermal methods. Diameters of these NWs were found to be in range of 5-200 nm, while their lengths achieved several tens μm.

Numerous experimental studies were accompanied by several *ab initio* calculations (using mainly the density functional theory) on the structural and electronic properties of nanowires

*Corresponding author: quantzh@latnet.lv

exhibited both the *ferroelectricity* ($BaTiO_3$ [13,14] and $PbTiO_3$ [15-17]) as well as the *photocatalytic* activity towards water splitting ($Bi_2Ti_2O_7$ [18], $SrTiO_3$ [19] and $CaTiO_3$ [20]). Initial shapes of ternary metal oxide NWs mentioned above corresponded to square cross-sections chosen as: (*i*) non-stoichiometric, symmetrically terminated by either AO or BO_2 facets ($PbTiO_3$ [15-17], $SrTiO_3$ [19], $CaTiO_3$ [20]), (*ii*) stoichiometric, terminated by either two pairs of adjoined AO and BO_2 facets ($BaTiO_3$ [13], $Bi_2Ti_2O_7$ [18]) or alternated AO and BO_2 facets ($Bi_2Ti_2O_7$ [18]), (*iii*) both non-stoichiometric and stoichiometric ($BaTiO_3$ [14]).

Photocatalytic H_2 production under solar light irradiation of aqueous electrolytes in a presence of semiconducting electrodes (*e.g.*, nanowires) might be a clean and renewable source for hydrogen fuel. Splitting of water molecules in this catalytic process generally involves four stages [21]: (*i*) generation of electrons and holes by photoexcitation; (*ii*) charge separation and migration of the photo-generated carriers to the surface; (*iii*) recombination of the photogenerated electron–hole pairs during migration; (*iv*) subsequent reduction/oxidation of the adsorbed reactants directly by electrons/holes or by reactive oxygen species. Efficiency of the water splitting reactions depends on both the semiconductor band gap width and the relative position of band gap edges (hole and electron energies) with respect to the redox (reduction or oxidation) levels, which are defined as measure of the affinity of the semiconducting substance for electrons (electronegativity) compared with hydrogen [22]. Photoelectrochemical reactions can be determined by molecules or ions in a solution reduced or oxidized by a pure electron transfer. This requires the semiconductors to have proper band alignment relative to the water redox potentials, *e.g.*, the bottom of conduction band (CB minimum) of the *p*-type photocathode should be higher than the reduction potential H^+/H_2, while the top of the valence band (VB maximum) of the *n*-type photoanode, should be lower than the oxidation potential O_2/H_2O [23]: $\varepsilon_{CB\_bottom} > \varepsilon_{H_2\_reduction} > \varepsilon_{O_2\_oxidation} > \varepsilon_{VB\_top}$. The width of band gap ($\Delta\varepsilon_{gap} = \varepsilon_{CB\_bottom} - \varepsilon_{VB\_top}$) can be regulated mainly by differently substituted dopants as well as vacancies, which made them to be fitted for visible-light range photocatalysis (within the energy range 1.23-2.50 eV [24]). Thereafter, positions of the edges of band gaps (ε_{CB_bottom} and ε_{VB_top}), which must correspond to correlation of energy levels, can be effectively changed by structural reconstruction [25]. Both experimental and theoretical studies suggest that the electron transfer between semiconductor surface and aqueous redox species can occur at their interface only when the two orbitals, one belonging to the semiconductor and a second one belonging to the aqueous species, are of similar energy [26].

Strontium titanate was well-known along ago as an effective catalyst for splitting H_2O molecules into H_2 and O_2 components in stoichiometric amounts in photoelectrode system consisting of two electrodes $SrTiO_3$ (anode) and Pt (cathode) in aqueous electrolytes with or without applied external potential [27]. Among the different semiconductors used as photocatalysts, $SrTiO_3$ is a promising material due to its thermal stability and high resistance against photocorrosion [28]. To increase specific areas of photoelectrodes and to modify their properties, they were mainly composed from $SrTiO_3$ powders or nanoparticles fixed at substrates [28-32]. Pristine powder is directly active photocatalyst for water splitting under ultraviolet (UV) irradiation only [32] whereas to achieve its visible-light sensitivity to solar irradiation, either chemical or structural modification of strontium titanate (or both together) must be done [28]. For example, $SrTiO_3$ doped by various metal species (Cr-Ta [28], Mn and noble metal dopants [29], Pt [30], Rh [31] and Cr-La [32]) were found to be a highly active photocathode for sacrificial H_2 evolution under solar irradiation. On the contrary, for effective O_2-evolving photocatalysis in the visible-light range, $BiVO_4$ and WO_3 photoanodes in the presence or absence of electron mediators were suggested [31]. In such a case, the two-step overall water splitting can be realized in the presence of suitable redox couple although for the latter, the two differently modified $SrTiO_3$ photoelectrodes were applied too (redox shuttle)

[28]. Not only $SrTiO_3$ powders and nanoparticles, but also arrays of Ag-doped $SrTiO_3$ nanotubes studied experimentally were found to be photocatalytically active too [33].

Strontium titanate nanowires have been synthesized a number of times during the last decade [1,6,9,11]. However, to the best of our knowledge, only two references on the experimental studies of their photocatalytic properties can be given: (*i*) mixed mesh film assembled from Ru-doped $SrTiO_3$ NWs and $BiVO_4$ NWs or mesh bilayer composed of the same types of nanowires (either Ru-doped $SrTiO_3$ or $BiVO_4$ NWs) separated between themselves [12], (*ii*) bundles of TiO_2 NWs covered by cubic $SrTiO_3$ nanoclusters each [34]. Diameters of these types of synthesized nanowires were found within the range from several tens up to 100-150 nm. The only theoretical study of $SrTiO_3$ NWs found so far in literature has been performed recently [19] using plane-wave DFT calculations on non-stoichiometric SrO- or TiO_2-terminated four-faceted nanowires described by D_{4h} point group and oriented along [001] crystallographic axis. Surface atoms of these nanowires result in appearance of the electronic states inside the band gaps of $SrTiO_3$ NWs. In TiO_2-terminated NWs, mid-band states induced by the combination of O and Sr atoms positioned on the facets shift the top of the VB toward the conduction band, thus reducing the band gap as compared to $SrTiO_3$ bulk. These states have not been found interfering with the CB bottom, which plays an essential role for determining the driving force of H_2 evolution. In contrary, the electronic states induced by the combination O and Sr atoms (positioned on the facets) shift the CB bottom toward the valence band which excludes application of this type of $SrTiO_3$ NWs for photocatalysis [19].

To verify results reported in Ref. [19] and to extend the notions on photocatalytic applications of strontium titanate nanowires in dependence on their structural and electronic properties, we have consequently performed in this study the large-scale periodic calculations based on the atomic orbital basis and hybrid exchange-correlation potential. We have simulated the structural and electronic properties of both stoichiometric and non-stoichiometric [001]-oriented four-faceted $SrTiO_3$ nanowires cut from cubic bulk structure. Their diameters have been varied from 0.3 up to 2.4 nm with a correspondence to a consequent change of NW cross-section from 1×1 to 5×5 extension of the lattice constant of bulk.

The paper is organized as follows. Atomistic models of both stoichiometric and non-stoichiometric $SrTiO_3$ NWs as well as details of methods to calculate their electronic and thermodynamic properties are discussed in Section 2. Main results obtained for optimized nanowires of different terminations and thicknesses are analyzed in Section 3. Discussion on possible photocatalytic applications of $SrTiO_3$ nanowires depending on their structure is given in Section 4 while the main conclusions are summarized in Section 5.

2. Theoretical background

2.1. Atomistic models of [001]-oriented $SrTiO_3$ nanowires

The symmetry of simple cubic (*sc*) structure for Ti-centered unit cell (UC) of $SrTiO_3$ bulk (Fig. 1) is described by the space group $Pm\bar{3}m$ (point group O_h). Square-shaped Ti-centered

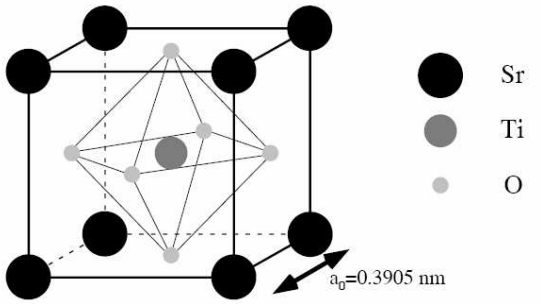

Figure 1. Axonometric image of *sc*-$SrTiO_3$ unit cell containing Ti atom in the center of the unit cell and six O atoms forming octahedron around it. Right panel contains labels of constituent atoms while arrow indicates the unit cell parameter a_o.

non-stoichiometric nanowire with the smallest thickness (1×1) cut from $SrTiO_3$ bulk can be considered as four-faceted [001]-oriented infinite prism, which unit cell with length a_o is terminated by lateral SrO-containing square facets of nanocube imaged in Fig. 1, since its lateral facets {100}, $\{\bar{1}00\}$, $\{0\bar{1}0\}$, and {010} possess the smallest surface energy among any other cubic STO facets. Analogously, non-stoichiometric (1×1) [001]-oriented STO NW can be constructed from Sr-centered bulk UC. In this study, we consider 3×3, 4×4, 5×5 SrO- or TiO_2-terminated and simultaneously Sr- or Ti-centered non-stoichiometric $SrTiO_3$ NWs (Figs. 2a-f), then optimize their geometry and calculate their properties. All these [001]-oriented nanowires can be described by D_{4h} point group, while for NWs axes, which contain O atoms only, the local symmetry is reduced to D_{2h} point group.

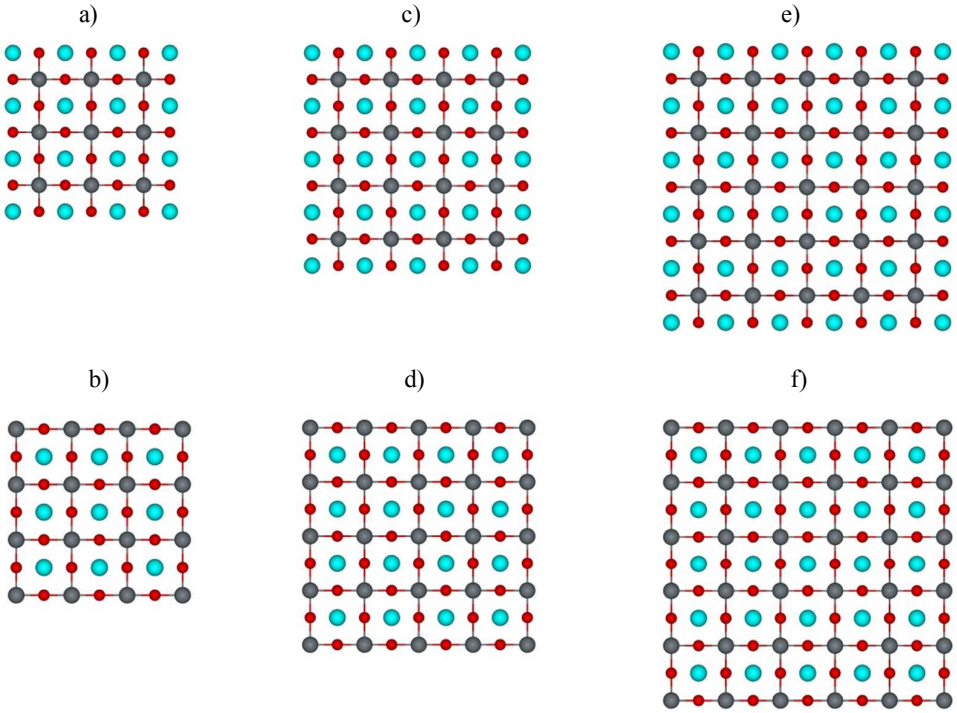

Figure 2. Cross sections of non-optimized structures for non-stoichiometric SrO- and TiO_2-terminated STO NWs with different thicknesses: 3×3 (a and b), 4×4 (c and d) as well as 5×5 (e and f), respectively. Sr and invisible O atoms (under Ti atoms) form a lower next-neighboring layer for each NW unit cell (according to space arrangement of atoms shown in Fig. 1).

In stoichiometric STO NW (Fig. 3), the two pairs of SrO-terminated and TiO_2-terminated adjoined facets form nanowire described by two mirror planes oriented along nanowire axis and cross-section diagonals so that C_{2v} point group represents the NW symmetry. Models of stoichiometric $SrTiO_3$ nanowires of different thicknesses (Fig. 4) have been constructed and calculated in this study as well. Geometry optimization has resulted in structural relaxation in proximity of NW corners.

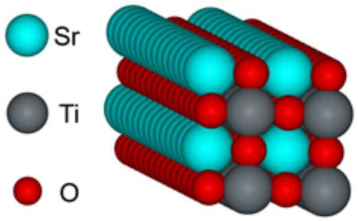

Figure 3. Axonometric image of stoichiometric [001]-oriented $SrTiO_3$ NW terminated by both SrO {100} and $\{0\bar{1}0\}$ as well as TiO_2 $\{\bar{1}00\}$ and {010} facets with 2×2 extension of the thinnest possible 1×1 nanowire (5 atoms *per* UC). Left panel contains labels of constituent atoms.

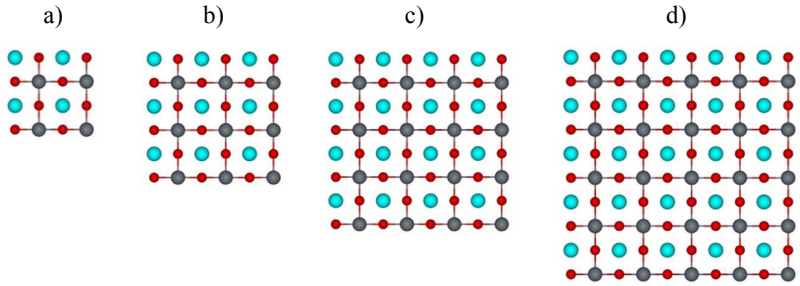

Figure 4. Cross sections of non-optimized structures of stoichiometric STO NWs with different thicknesses: a) 2×2, b) 3×3, c) 4×4, d) 5×5. Sr and invisible O atoms (under Ti atoms) form a lower next-neighboring layer for each NW unit cell (Fig. 1).

2.2. Computational details

Ab initio calculations on [001]-oriented $SrTiO_3$ nanowires of different diameters described above, both non-stoichiometric and stoichiometric, have been performed within the periodic hybrid DFT-LCAO method, which utilizes localized Gaussian-type functions (GTFs) in the form of basis set (BS) for expansion of crystalline orbitals as linear combinations of atomic orbitals, implemented in *CRYSTAL14* computer code [35] using exchange–correlation functional PBE0 [36,37] with 16% contribution of Hartree-Fock (HF) exchange. The all-electron basis set 6*s*-311*sp*-1*d* has been chosen for O atoms [38], while both the small-core relativistic effective core potentials (ECPs) and the corresponding BSs have been applied for Sr 111*s*-111*p*-1*d* [39] and Ti 11111*s*-111111*p*-11111*d* [40] which include sub-valence, valence and virtual orbitals. For optimization of O, Sr and Ti basis sets performed recently for STO bulk [41] using original program OPTBAS [42], the Powell's conjugate directions minimization method [43] has been applied. To exclude BS linear dependence in LCAO crystal calculations, the diffuse *s*-, *sp*-, *p*- and *d*-orbitals with exponents less than 0.1 have been removed from the corresponding basis sets. As a result, the optimized lattice constant of cubic STO bulk (Fig. 1) has been found to be different from the experimental value by less than 1% [41].

The Brillouin zone for 3D cubic $SrTiO_3$ crystal has been sampled using Monkhorst–Pack 12×12×12 *k*-point mesh [44]. For 1D STO NWs, this *k*-mesh has been reduced to 12×1×1 correspondingly. Tolerance of the energy convergence on the self-consistent field (SCF) cycles has been set to 10^{-8} a.u. (an extra-large pruned DFT integration grid has been adopted). Both spin-restricted and spin-polarized calculations on $SrTiO_3$ nanowires have been performed in the current study, the latter are especially important for non-stoichiometric nanowires. To evaluate the Coulomb and exchange series appearing in the SCF equations for periodic systems, five tolerances have been controlled: 10^{-9}, 10^{-9}, 10^{-9}, 10^{-9} and 10^{-18} (related to estimates of overlap or penetration for integrals of Gaussian functions on different centers, which define cutoff limits for series summation). The full structural optimization has been performed for all aforementioned configurations of STO NWs (Figs. 2,4). Prismatic nanowires of chosen orientation and Miller indices of their lateral facets have been generated using keyword NANOROD implemented recently in *CRYSTAL14* code [35].

2.3. Formation energy of stoichiometric and non-stoichiometric $SrTiO_3$ nanowires

The formation energy for stoichiometric and non-stoichiometric $SrTiO_3$ nanowires can be calculated within the unified approach using the chemical potential formalism. Let firstly consider the composition of the nanowires. The stoichiometric $SrTiO_3$ nanowires (Fig. 4) comprise the entire number of the bulk unit cells. For $n\times n$ NWs the number of STO formula units (FU) is n^2. In symmetric non-stoichiometric $SrTiO_3$ NWs of size $n\times n$ (Fig. 2), the overall

NW composition can be represented as $(TiO_2)_k(Ti_2O_3)_l(SrO)_m$ where k, l, and m are the integer numbers uniquely determined by the value of n and the type of the termination:

$$\begin{array}{llll} k = n^2 + 2n - 1 & & k = n^2 - 2 & \\ l = 1 & \textit{for } TiO_2\textit{-terminated NW}; & l = 1 & \textit{for SrO-terminated NW}. \\ m = n^2 & & m = (n+1)^2 & \end{array} \quad (1)$$

The concrete values of k, l, and m for non-stoichiometric STO NWs are considered in Table 1.

The formation energy ΔG_{form} of any object is defined in thermodynamics as the excess (free) energy in order to form an object from the substances i taken from the reservoir with chemical potential μ_i:

$$\Delta G_{\text{form}} = G - \sum_i N_i \mu_i. \quad (2)$$

This definition obviously depends on the set of substances i chosen. Frequently, the separated atoms in the gas phase, or atoms in the elementary substance (solid/gas) are represented as the reference set. However, both those choices are not well applied to NW systems, mainly because of the relatively low accuracy of the energies calculated for isolated atoms and metallic phases using the LCAO basis set chosen. Also, in this case the difference between two terms in the right side of Eq. (2) can reach several tens of eV, which may lead to additional accuracy loss. Moreover, the coexistence of perovskite phases with Sr or Ti atoms in the gas phase or with Sr metallic phase can hardly be realized. Due to these reasons, we have selected subunits TiO_2, Ti_2O_3 and SrO as the reference constituents for calculation of the formation energies of $SrTiO_3$ NWs. This approach is similar to that used by Padilla and Vanderbilt in their study of $SrTiO_3$ surfaces [45]. Consequently, to calculate the NW formation energy we use the following equation:

$$\Delta G_{\text{form}}(\text{NW}) = G(\text{NW}) - k\mu_{\text{TiO}_2} - l\mu_{\text{Ti}_2\text{O}_3} - m\mu_{\text{SrO}}. \quad (3)$$

The stable oxide phases are considered as the reference states of subunits:

$$\mu_{\text{X}} = G^0_{\text{X}} + \Delta\mu_{\text{X}}, \quad (4)$$

where G^0_{X} is the molar (free) energy of the corresponding bulks (X = TiO_2, Ti_2O_3, SrO). In the oxygen atmosphere, the TiO_2 and Ti_2O_3 species are not independent, and we should take into account the equilibrium between them: $2\text{TiO}_2 \leftrightarrow \text{Ti}_2\text{O}_3 + \frac{1}{2}\text{O}_2$. Thus, instead of TiO_2, Ti_2O_3 and SrO components we can consider the substances TiO_2, O_2 and SrO, and substitute $\Delta\mu_{\text{Ti}_2\text{O}_3}$ by $\Delta\mu_{\text{TiO}_2}$ as follows:

$$\Delta\mu_{\text{Ti}_2\text{O}_3} = 2\Delta\mu_{\text{TiO}_2} + 2G^0_{\text{TiO}_2} - G^0_{\text{Ti}_2\text{O}_3} - \frac{1}{2}\mu_{\text{O}_2}. \quad (5)$$

The chemical potential of the gaseous O_2 (μ_{O_2}) can be introduced in the following form [46]:

$$\begin{aligned} \mu_{\text{O}_2}(T,P) &= E_{\text{O}_2} + \Delta\mu_{\text{O}_2}(T,P); \\ \Delta\mu_{\text{O}_2}(T,P) &= \Delta\mu_{\text{O}_2}(T,P_0) + kT\ln\frac{P}{P_0}, \end{aligned} \quad (6)$$

where E_{O_2} is the total (electronic) energy of the isolated oxygen molecule at $T = 0$ K, P_0 is the standard atmospheric pressure (1 bar), and $\Delta\mu_{\text{O}_2}(T,P_0)$ contains all temperature dependent free energy contributions at $P = P_0$ tabulated in standard thermochemical data tables [47].

Assuming the equilibrium of the nanowire with its own bulk,

$$\begin{gathered}\mu_{TiO_2}+\mu_{SrO}=\mu_{SrTiO_3}=G^0_{SrTiO_3};\\ \Delta\mu_{TiO_2}+\Delta\mu_{SrO}=G^0_{SrTiO_3}-G^0_{TiO_2}-G^0_{SrO}=\Delta G_{SrTiO_3},\end{gathered} \tag{7}$$

and taking into account Eqs. (4–7), we can rewrite the Eq. (3) as follows:

$$\begin{gathered}\Delta G_{form}(NW)=G(NW)-(k+2l-m)G^0_{TiO_2}-mG^0_{SrTiO_3}+\frac{l}{2}E_{O_2}-\\ -(k+2l-m)\Delta\mu_{TiO_2}+\frac{l}{2}\Delta\mu_{O_2}(T,P).\end{gathered} \tag{8}$$

Under an equilibrium condition, the chemical potential can admit a limited value. For the thermodynamically stable STO NW, the variations of chemical potentials are restricted by possible NW disintegration due to formation of competing phases such as TiO_2, Ti_2O_3, and SrO. The extreme reduction conditions correspond to equilibrium between NW and Ti_2O_3 phase ($\Delta\mu_{Ti_2O_3}=0$). Using Eq. (8), we can obtain the NW formation energies for TiO_2-Ti_2O_3-rich point ($\Delta\mu_{TiO_2}=0$):

$$\Delta G_{form}(NW)=G(NW)-(k-m)G^0_{TiO_2}-lG^0_{Ti_2O_3}-mG^0_{SrTiO_3}, \tag{9}$$

and for SrO-Ti_2O_3-rich point ($\Delta\mu_{TiO_2}=0$):

$$\Delta G_{form}(NW)=G(NW)-kG^0_{SrTiO_3}-lG^0_{Ti_2O_3}-(m-k)G^0_{SrO}. \tag{10}$$

Basic DFT-LCAO calculations cannot give Gibbs free energy including entropy of vibration without additional methodology like frozen phonon method [48] which is out of scope of the present study. It may be assumed [45,49] that the entropy and volume contributions to the energy differences in Eqs. (8), (9), and (10) are not large enough. Based on this assumption, the total energy E_X of solid phase X obtained in DFT LCAO simulations is allowed to be substituted for Gibbs free energy of the corresponding phase, *i.e.*, in first approximation $G^0_X=E_X$. To estimate formation energies, the total energies of bulk TiO_2, Ti_2O_3, SrO and isolated O_2 molecule have been obtained within the same computational approach as specified in Subsection 2.2. Spin-polarized calculations have been performed for Ti_2O_3 bulk and isolated O_2 molecule.

In Table 1, we present the reduced formation energies $\Delta\overline{E}_{form}=2\Delta G_{form}/(k+l+m)$ calculated for non-stoichiometric NWs at TiO_2-Ti_2O_3-rich and SrO-Ti_2O_3-rich conditions. The scale factor $(k+l+m)/2$, which is the same for TiO_2- and SrO-terminated NWs, provides the proper comparison between both types of non-stoichiometric terminations and with stoichiometric NWs (see discussion below). Table 1 also shows that the content of Ti_2O_3 subunits is small and constant (l = 1) in all the nanowires considered. Maximal stability at reduction condition is found for the SrO-terminated NWs in SrO-rich region.

In the stoichiometric case ($k = m = n^2$, $l = 0$), Eqs. (8), (9), and (10) turn into the trivial form which does not depend on chemical potentials mentioned above, and the reduced formation energies can be calculated as usually:

$$\Delta\overline{E}_{form}(NW)=E(NW)/n^2-E_{SrTiO_3}. \tag{11}$$

Table 1. Reduced formation energy of non-stoichiometric $SrTiO_3$ NWs at reduction conditions.

Nanowire	k	l	m	$\frac{(k+l+m)}{2}$	$\Delta\overline{E}_{\text{form}}$, kJ/mol		
					TiO_2-rich	SrO-rich	averaged*
TiO_2-terminated							
3×3	14	1	9	12	119	189	154
4×4	23	1	16	20	95	154	125
5×5	34	1	25	30	79	129	104
SrO-terminated							
3×3	7	1	16	12	218	92	155
4×4	14	1	25	20	161	68	115
5×5	23	1	36	30	127	54	91

*The average between TiO_2- and SrO-rich values is given for comparison with stoichiometric NW results (Table 2).

Table 2. Reduced formation energy of stoichiometric $SrTiO_3$ nanowires.

Nanowire	Number of formula units *per* unit cell	$\Delta\overline{E}_{\text{form}}$, kJ/mol
bulk	1	0
1×1	1	508
2×2	4	263
3×3	9	178
4×4	16	134
5×5	25	108

Formation energies of stoichiometric $SrTiO_3$ NWs calculated using Eq. (11) are given in Table 2. Comparison of these values with averaged values for non-stoichiometric $SrTiO_3$ NWs, given in the last column of Table 1, shows that both cases exhibit similar stability at reduction conditions. More information can be achieved from the analysis of formation energy dependence on the chemical potentials. In Fig. 5, we show the dependence of reduced formation energy for 4×4 NWs on TiO_2 chemical potential $\Delta\mu_{TiO_2}$ at T= 298.15 K and $P_{O_2} = P_0$ calculated using Eqs. (8) and standard thermodynamic data [47] for the oxygen gas phase. The TiO_2 chemical potential is allowed to vary over the range: $0 \geq \Delta\mu_{TiO_2} \geq \Delta G_{SrTiO_3}$. As expected,

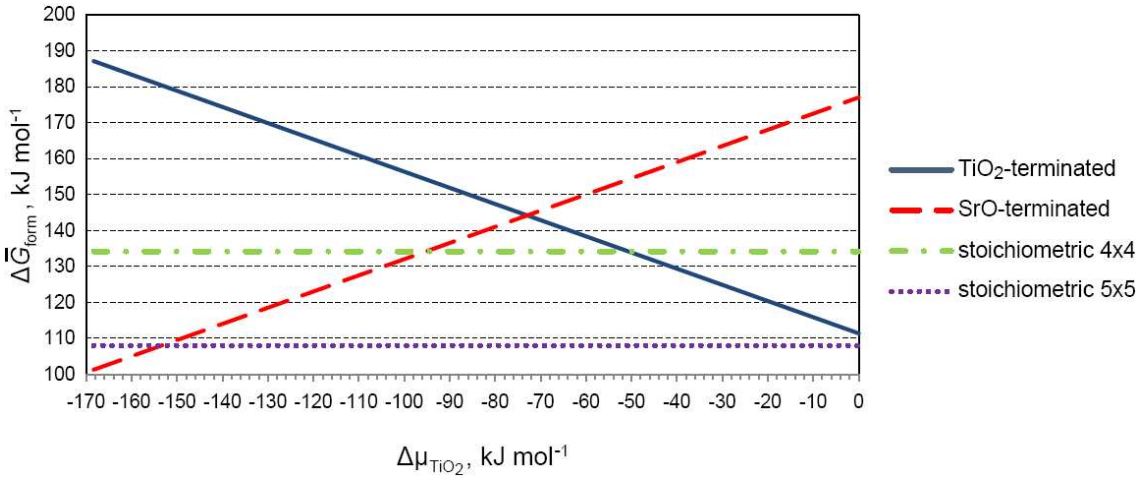

Figure 5. Reduced formation energy of non-stoichiometric TiO_2- and SrO-terminated 4×4 (Fig. 2) as well as stoichiometric 4×4 and 5×5 (Fig. 4) $SrTiO_3$ nanowires *vs.* TiO_2 chemical potential $\Delta\mu_{TiO_2}$ is considered at T = 298.15 K and $P_{O_2} = P_0$.

the TiO_2-terminated $SrTiO_3$ nanowires is more stable at TiO_2-rich conditions whereas the SrO-terminated NW more stable at SrO-rich conditions. For comparison, we depict the horizontal lines corresponding to 4×4 and 5×5 stoichiometric $SrTiO_3$ nanowires. This clearly shows that at low values of n the stoichiometric nanowires are more favorable than non-stoichiometric nanowires in the middle range of $\Delta\mu_{TiO_2}$. However, the SrO-terminated nanowires are found to be preferable in SrO-rich region (as follows from the left area of Fig. 5).

As mentioned above, present calculations on $SrTiO_3$ nanowires cannot provide the strict description of dependence of their formation energy on pressure and temperature, unlike their evident dependence on NW diameter. However, the analysis of oxygen gas phase contribution demonstrates that those terms have a relatively low influence on the calculated formation energies, due to the low fraction of Ti_2O_3 subunits (l = 1) in overall nanowire composition. Indeed, contribution of the temperature-dependent term estimated at 1000 K is equal to 5 kJ/mol. The sign of these contributions is the same for TiO_2- and SrO-terminated NWs. Growth of the oxygen pressure reduces the stability of non-stoichiometric nanowires and does not affect the stability of stoichiometric nanowires.

3. Main electronic properties of $SrTiO_3$ nanowires

3.1. Non-stoichiometric STO NWs

While Table 1 describes the dependence of formation energies for various non-stoichiometric $SrTiO_3$ nanowires on their terminations and thicknesses, then Table 3 gives for them the optimized values of NW diameters d_{NW} and UC lengths l_{NW_UC} as well as "band gap" widths $\Delta\varepsilon_{gap}$ defined as $\varepsilon_F - \varepsilon_{VB\_top}$, *i.e.*, differences of the Fermi levels crossing the conduction bands (Fig. 6) and the tops of the corresponding valence bands. Obviously, $\Delta\varepsilon_{gap}$ here is not a regular band gap because it corresponds to a distance between the occupied states. We discuss only results of spin-polarized calculations on the non-stoichiometric STO NWs with SrO and TiO_2 terminations as more realistic for systems with non-zero total spin moment.

Table 3. Geometry and band structure of non-stoichiometric STO NW *vs.* termination and thickness.

Nanowire	d_{NW} (Δd_{NW}[a]), nm	l_{NW_UC} (Δl_{NW_UC}[a]), nm	$\Delta\varepsilon_{gap}$[b], eV	ε_F, eV	ε_{VB_top}[b], eV
SrO-terminated					
3×3	1.57 (-0.09)	0.387 (-0.004)	3.92	1.32	-2.60
4×4	2.12 (-0.10)	0.388 (-0.003)	3.60	0.94	-2.65
5×5	2.67 (-0.10)	0.389 (-0.003)	3.34	0.69	-2.65
TiO_2-terminated					
3×3	1.74 (0.08)	0.374 (-0.017)	3.18	-3.09	-6.27
4×4	2.28 (0.07)	0.379 (-0.012)	2.74	-3.30	-6.03
5×5	2.83 (0.06)	0.382 (-0.009)	2.50	-3.42	-5.91

[a] Δd_{NW} and Δl_{NW_UC} are changes of diameters and UC lengths as compared to non-optimized NWs,
[b] values of $\Delta\varepsilon_{gap}$ and ε_{VB_top} calculated for STO bulk: 3.08 and -4.00 eV, respectively.

Analogously to rutile-phase TiO_2 NWs of different orientations and terminations calculated by us previously using the same DFT-LCAO PBE0 Hamiltonian [50], dependences of Δd_{NW} and Δl_{NW_UC} on TiO_2-terminated $SrTiO_3$ NW thicknesses are found to be qualitatively similar, *i.e.*, the larger is the NW diameter the smaller an increase of d_{NW} and decrease of Δl_{NW_UC} as compared to those in non-optimized NW structures. In contrary, d_{NW} of SrO-terminated $SrTiO_3$ nanowires decreases with the growth of thickness, although such a reduction is slowed down with larger values of diameter while Δl_{NW_UC} is reduced down to UC length for non-

optimized NW structure. It means that the structural parameters of STO NW approach to those in correspondingly sectioned $SrTiO_3$ crystal with increase of d_{NW}. In particular, a length of NW unit cell approaches to bulk unit cell parameter a_0 (Fig. 1). Obviously these results correlate with decrease of formation energies $\Delta\overline{E}_{form}$ depending on increase of d_{NW} (Table 1) confirming a growth of NW stability with enlarging thickness.

The NW band widths decrease for both SrO- and TiO_2-terminated $SrTiO_3$ nanowires with growing values of d_{NW} for 3×3, 4×4 and 5×5 thicknesses (Fig. 2) although values of $\Delta\varepsilon_{gap}$ of the former are essentially larger than those in bulk (Table 3). Meanwhile, as compared to the band structures of non-stoichiometric 4×4 STO nanowires calculated earlier by plane wave DFT method [19], those obtained in the current study (Figs. 6a,b) looks noticeably different. One of the most important differences is observed for $\Delta\varepsilon_{gap}$ values which are essentially underestimated when using standard plane wave DFT methods, unlike hybrid DFT+HF LCAO method *PBE0* used by us. Moreover, essential differences can be observed in band distributions for both SrO- and TiO_2-terminated nanowires when using both first principle approaches. The band structure of Sr-terminated STO NW obtained in Ref. [19] contains a deep explicit energy level inside the gap chipped off the CB bottom. Such a level has not been observed in our calculations at all (Fig. 6a and Fig. *SI*1a in Supplementary Information). The shallow explicit band below the bottom of CB of TiO_2-terminated STO NW (Fig. 6b and Fig. *SI*1b in Supplementary Information) has been found in our study to be completely populated. Most important result of our calculations is that the Fermi levels ε_F cross the CB bottoms for both terminations of STO NWs, *i.e.*, a few virtual bands are partly populated and NWs become conducting. Therefore, aforementioned factors explain why the real values of inter-band gaps $\Delta\varepsilon_{gap}$ obtained in the current study essentially exceed the band gaps discussed in Ref. [19].

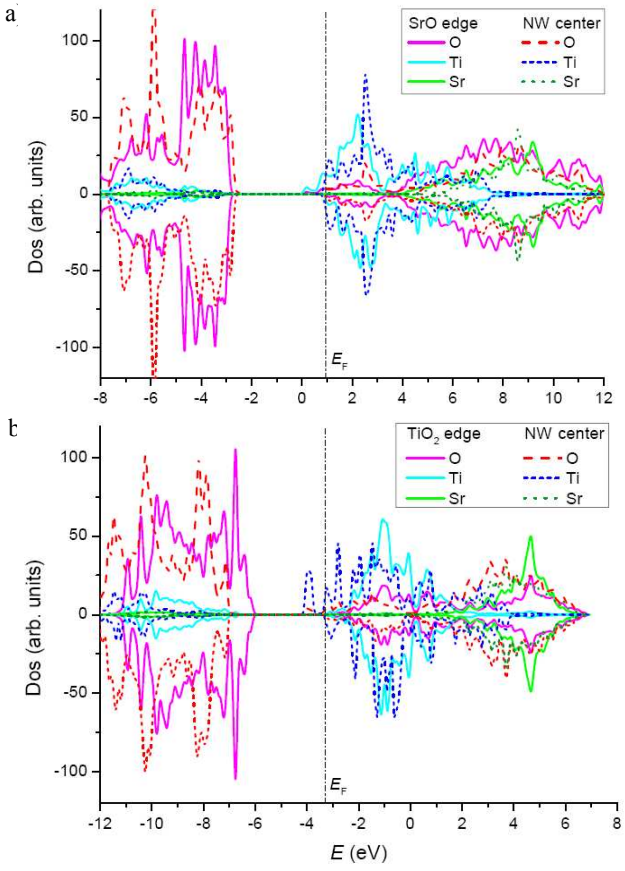

Figure 6. Projected densities of states (PDOSs) for different atoms and areas (as shown in both insets) of non-stoichiometric 4×4 STO nanowires: SrO-terminated (a) and TiO_2-terminated (b).

For different types of atoms positioned at either edges or centers of $SrTiO_3$ nanowires, their PDOSs are present for both SrO- and TiO_2-terminated STO NWs (Figs. 6a,b, respectively). In both cases, the bottoms of the conduction bands are crossed by the Fermi levels, thus increasing $\Delta\varepsilon_{gap}$ values. In the former case, the top of the VB is predominantly composed of O(2*p*) spin-paired states at both NW center and facets while the bottom of the CB is mainly composed of Ti(3*d*) spin-unpaired states of outmost titanium atoms particularly accompanied by surface O(2*p*) states too (Fig. 6a). On the contrary, the top of the valence band in non-stoichiometric NWs with TiO_2 terminations is composed of O(2*p*) spin-paired states of oxygen atoms located on TiO_2-terminated facets (edges), while the bottom of the conduction band contains mainly Ti(3*d*) spin-unpaired states of titanium atoms at the NW center (Fig. 6b). These results clearly exhibit predominance of Ti(3*d*)–O(2*p*) bonds possessing ionic-covalent nature as compared to evidently ionic Sr(5*s*)–O(2*p*) bonds although the latter binding type affects the electronic structure of both types of non-stoichiometric NWs, which well correlates with the conclusion drawn in Ref. [19]. As to the populated explicit levels of STO NWs located at the vicinity of the bottom of the conduction band for the SrO-terminated nanowire, they mainly consist of edge states (Fig. 6a), while the explicit level of TiO_2-terminated NW is composed mainly of spin-unpaired Ti(3*d*) and partly O(2*p*) states generated by NW central atoms (Fig. 6b). The latter results can witness on local NW conductivity at surface *vs.* center areas of SrO- or TiO_2-terminated nanowires, respectively.

Table 4. Mulliken charges of atoms (*e*) in centers and at edges of non-stoichiometric STO NWs.

Nanowire	NW center			SrO edge			TiO_2 edge		
	q_{Sr}	q_{Ti}	q_O*	q_{Sr}	q_{Ti}	q_O*	q_{Sr}	q_{Ti}	q_O*
SrO-terminated									
3×3	1.95	2.28	-1.46 -1.46	1.85	2.22	-1.54 -1.66			
4×4	1.95	2.28	-1.43 -1.44	1.85	2.22	-1.54 -1.65			
5×5	1.95	2.28	-1.42 -1.42	1.85	2.23	-1.53 -1.65			
TiO_2-terminated									
3×3	1.95	2.19	-1.46 -1.40	–	–	– –	1.94	2.09	-1.24 -1.17
4×4	1.95	2.22	-1.45 -1.42	–	–	– –	1.94	2.09	-1.23 -1.19
5×5	1.95	2.24	-1.44 -1.41	–	–	– –	1.94	2.09	-1.23 -1.19

* The upper value is for O ion in TiO_2 atomic plane, and the lower value is for O ion in SrO atomic plane.

Results discussed when analyzing PDOS states are well-correlated with the values of the effective charges q_O, q_{Sr} and q_{Ti} calculated in both NW centers and at their edges (Table 4). Except for edges of SrO-terminated NWs, in other nanowire configurations, strontium ion is very close to pure ionic Sr^{2+} state, which practically excludes any Sr involvement in covalent bonding. Effective charges of titanium and especially oxygen ions are much more sensitive to their arrangement in nanowires, for example, O ionicity reduces when the oxygen positions change from the edges of SrO-terminated nanowires to the edges of TiO_2-terminated STO NWs. For the fixed arrangement of oxygen or titanium ions, their effective charges have been found to be almost insensitive on value of d_{NW}.

3.2. Stoichiometric STO NWs

Unlike non-stoichiometric nanowires, Fig. 5 clearly demonstrates independence of the formation energies for stoichiometric $SrTiO_3$ NWs on TiO_2 chemical potential, keeping dependence on their thickness only. Moreover, 1×1 stoichiometric $SrTiO_3$ NW is found to be energetically too unstable as compared to more thick nanowires (Table 2), and we do not consider this ultrathin NW configuration anymore. Table 5 describes the optimized values of d_{NW}, l_{NW_UC}, $\Delta\varepsilon_{gap}$, ε_{CB_bottom} and ε_{VB_top} for stoichiometric nanowires, analogously to Table 3 in previous Subsection. Since the total spin moment of stoichiometric $SrTiO_3$ NWs is zero, the spin-restricted DFT-LCAO calculations of their properties have been performed. Similarly to SrO-terminated STO NWs (Table 3), both d_{NW} and l_{NW_UC} decrease with growing $SrTiO_3$ NW thicknesses as compared to those in non-optimized NW structures. It means that the structural parameters of nanowire approach to those in correspondingly sectioned $SrTiO_3$ crystal with increase of d_{NW}. In particular, a length of NW unit cell approaches to bulk unit cell parameter a_0 (Fig. 1). Obviously, these results correlate with decrease of the formation energies $\Delta\overline{E}_{form}$ while d_{NW} increases (Table 1) confirming a growth of NW stability with enlarging thickness.

Table 5. Geometry and band structure of stoichiometric STO NW depending on its thickness.

Nanowire	d_{NW} (Δd_{NW}[a]), nm	l_{NW_UC} (Δl_{NW_UC}[a]), nm	$\Delta\varepsilon_{gap}$[b], eV	ε_{CB_bottom}[b], eV	ε_{VB_top}[b], eV
2×2	0.82 (-0.01)	0.379 (-0.012)	3.04	-1.60	-4.64
3×3	1.37 (-0.01)	0.381 (-0.010)	2.41	-1.82	-4.23
4×4	1.92 (-0.02)	0.384 (-0.007)	2.15	-1.92	-4.07
5×5	2.47 (-0.02)	0.386 (-0.006)	2.01	-1.99	-4.00

[a] Δd_{NW} and Δl_{NW_UC} are changes of diameters and UC lengths as compared to non-optimized NWs,
[b] values of $\Delta\varepsilon_{gap}$, ε_{CB_bottom} and ε_{VB_top} calculated for STO bulk: 3.08, -0.92 and -4.00 eV, respectively,

As to the band gaps of $SrTiO_3$ nanowires, their widths are consequently reduced (Table 5) with growing NW thicknesses (2×2, 3×3, 4×4 and 5×5 as shown in Fig. 4). Moreover, unlike partial conductivity of non-stoichiometric $SrTiO_3$ nanowires observed in our calculations (Fig. 6), their stoichiometric counterparts remain semiconducting irrespectively on the value of d_{NW}, *i.e.,* the width of band gap can be defined as usually: $\Delta\varepsilon_{gap} = \varepsilon_{CB\_bottom} - \varepsilon_{VB\_top}$ (Fig. 7). Analogously to both types of non-stoichiometric nanowires, the band gap remains non-direct since the CB bottom is achieved at Γ point of the BZ, whereas the VB top corresponds to Z point (Fig. *SI*2 in Supplementary Information). Values of $\Delta\varepsilon_{gap}$ are noticeably smaller than those for TiO_2-terminated $SrTiO_3$ nanowires and markedly smaller as compared to SrO-terminated STO NWs when comparing those for close values of d_{NW} (*cf.* Tables 3 and 5).

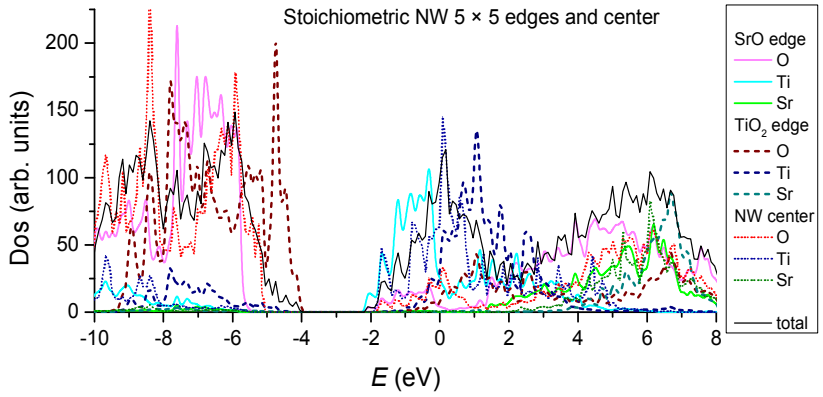

Figure 7. Projected densities of states (PDOSs) for different atoms and areas (as shown in inset) of stoichiometric 5×5 $SrTiO_3$ nanowire.

Analysis of Fig. 7 indicates that in stoichiometric STO NWs, the top of valence band is predominantly composed of O(2*p*) states from the edge oxygen atoms on TiO_2-terminated facets while the bottom of the conduction band is composed of Ti(3*d*) states from the outmost Ti atoms in SrO-terminated facets (Fig. 3). Contribution from central NW atoms as well as Sr atoms is practically neglecting for both edges of band gap which essentially differs from the case of non-stoichiometric STO NWs, where influence of central atoms is essentially large which can be explained by different morphology of both types of nanowires (*cf.* Figs. 2 and 4).

Table 6. Mulliken effective charges of atoms (*e*) in stoichiometric $SrTiO_3$ nanowires

Nanowire	NW center			SrO edge			TiO_2 edge		
	q_{Sr}	q_{Ti}	q_O*	q_{Sr}	q_{Ti}	q_O*	q_{Sr}	q_{Ti}	q_O*
2×2	–	–	–	1.85	2.21	-1.52 -1.55	1.94	2.07	-1.25 -1.20
3×3	1.95	2.25	-1.40 -1.37	1.85	2.24	-1.52 -1.59	1.94	2.08	-1.24 -1.20
4×4	1.95	2.26	-1.40 -1.36	1.85	2.24	-1.52 -1.60	1.94	2.08	-1.23 -1.21
5×5	1.95	2.28	-1.41 -1.40	1.85	2.24	-1.52 -1.61	1.94	2.08	-1.23 -1.21

* The upper value is for oxygen in TiO_2 atomic plane, and the lower value is for oxygen in SrO atomic plane.

Distribution of the effective charges in STO NWs is presented in Table 6, they can be compared with both PDOS plot (Fig. 7) and analogous values for non-stoichiometric nanowires (Table 4). Again, except for edges of SrO-terminated NW facets, strontium ion in other nanowire configurations can be attributed to pure ionic Sr^{2+} state, which practically excludes any Sr involvement in covalent bonding. Analogously to non-stoichiometric NWs, O ionicity reduces from positions at edges of SrO-terminated NW facets down to that in proximity of edges at TiO_2-terminated facets while the effective charge of central oxygen ions can be considered as averaged between those for edge atoms (*cf.* Tables 4 and 6). Similar conclusion can be drawn on insensitivity of the effective charges on oxygen or titanium ions on value of d_{NW} for their fixed arrangement in both non-stoichiometric and stoichiometric nanowires.

4. Suitability of regular $SrTiO_3$ nanowires for photocatalytic applications

On the basis of the standard thermodynamic conditions for H_2O molecule splitting, we discuss and evaluate the influence of cubic STO NW morphology on the photocatalytic activity of [001]-oriented non-stoichiometric and stoichiometric nanowires possessing different faceting and thickness (Figs. 2-4). We perform comparison of the band edge positions and Fermi levels with those for perfect $SrTiO_3$ bulk as well as with levels of reduction H^+/H_2 and oxidation O_2/H_2O potentials. Fig. 8 presents the energy diagram drawn using results discussed in Section 3, which allows one to estimate eligibility of all the types of strontium titanate nanowires considered here for photocatalytic applications.

The first energetic criterion of material suitability as photoelectrode is a proper ratio between its band gap edges as well as the potentials of reduction (H^+/H_2) and oxidation (O_2/H_2O) for water splitting reaction under solar irradiation is: $\varepsilon_{CB\_bottom} > \varepsilon_{H_2\_reduction} > \varepsilon_{O_2\_oxidation} > \varepsilon_{VB\_top}$ [23]. On the other hand, the band gap width of potential photoelectrode must correlate with the energy range of visible light spectrum between the infrared and ultraviolet regions of electromagnetic irradiation which is fitting for H_2O molecule dissociation, *i.e.*, 1.23 eV < $\Delta\varepsilon_{gap}$ < 2.50 eV [24]. Although structural reconstruction of the

corresponding material can provide necessary correlation of ε_{VB_top}, $\Delta\varepsilon_{gap}$ and ε_{CB_bottom} [25], the proper choice of potential candidates according to both criteria has to be done first.

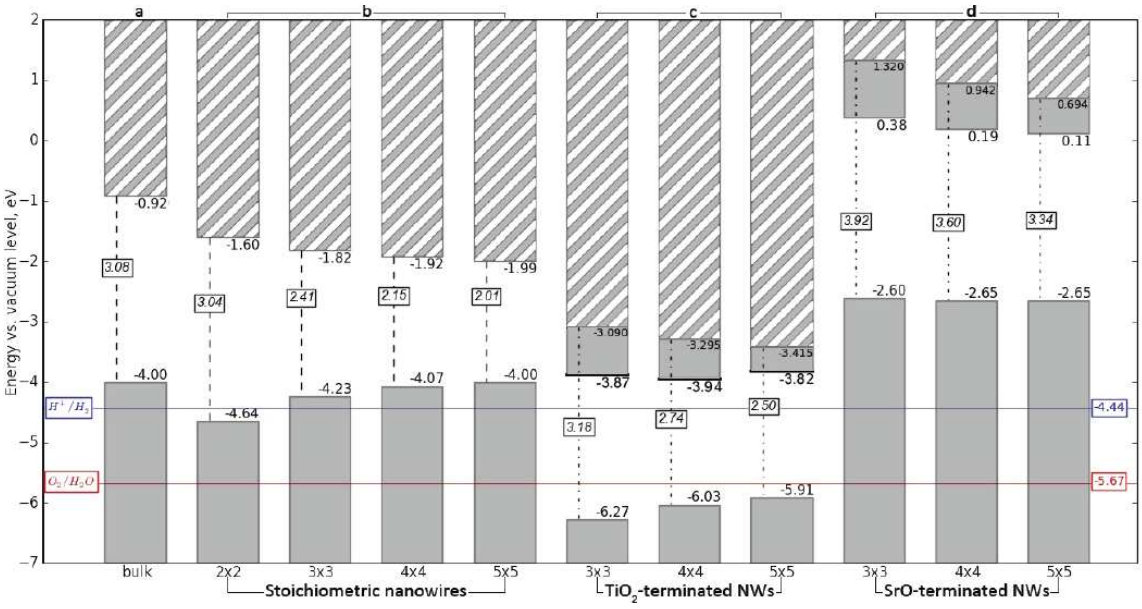

Figure 8. Energy diagram of the band structures of $SrTiO_3$ bulk as well as [001]-oriented stoichiometric and non-stoichiometric nanowires (Figs. 2-4) in proximity of the inter-band gap edges and redox potentials for H_2O molecule dissociation. Striped areas of columns consist of the virtual (non-populated) energy levels in the band structure unlike filled areas, the levels in which are populated.

Obviously, for [001]-oriented 3×3, 4×4 and 5×5 stoichiometric $SrTiO_3$ nanowires, the second criterion is fulfilled (Fig. 8), the same is certainly true for more thick nanowires, 6×6, 7×7, *etc*. However, the alignment criterion of band gap edges with redox potentials is rather far from realization for stoichiometric $SrTiO_3$ nanowires, at least the strategy of the corresponding structural reconstruction is not clear. Much closer for both aforementioned criteria are non-stoichiometric TiO_2-terminated STO NWs (Fig. 8), especially 5×5 and more thick nanowires (2.50 eV corresponds to energy of "violet" photon). However, our calculations have shown that non-stoichiometric $SrTiO_3$ nanowires rather possess local conductivity: SrO-terminated NWs possess it in areas of facets, whereas TiO_2-terminated NWs in the center. Thus, the latter can be considered as possible candidates for nanophotoelectrodes since the surface areas of these nanowires can be described as semiconductors whereas transition of the electron from the VB towards the CB can initiate dissociation of H_2O molecule under influence of visible light. Meanwhile, this result confirms conclusion drawn in Ref. [19] on suitability of TiO_2-terminated STO NWs for photocatalytic applications. As to SrO-terminated $SrTiO_3$ nanowires, Fig. 8 clearly demonstrates that they cannot be applied as photoelectrodes since both energy criteria are not fulfilled in this case.

5. Summary

We have performed comprehensive first-principles simulations of a few thin [001]-oriented $SrTiO_3$ NWs, both non-stoichiometric (either SrO- or TiO_2-terminated) and stoichiometric, diameters of which have been varied from 0.3 up to 2.4 nm. The current study can be considered as the first step in development of NW models for photocatalytic applications, the next steps will include implementation of vacancies and dopants in nanowires as has been done for $SrTiO_3$ nanotubes [51]. To estimate stability of these nanostructures, we have

calculated their formation energies $\Delta\overline{E}_{form}$, according to approximate thermodynamic formalism. Dependence of Gibbs energies $\Delta\overline{G}_{\text{form}}$ of non-stoichiometric STO NWs on chemical potential of TiO_2 formula unit $\Delta\mu_{TiO_2}$ has been shown, while stoichiometric NWs are insensitive to $\Delta\mu_{TiO_2}$. Irrespectively on nanowire termination, growth of NW thickness reduces its formation energy.

Hybrid DFT-LCAO calculations have shown that the values of $\Delta\varepsilon_{\text{gap}}$ for $SrTiO_3$ NWs of different structural types are consistently reduced with the growth of NW diameter although character of such a decrease depends on morphology of nanowire. Stoichiometric STO NWs are found to be semiconducting irrespectively on their thickness, while non-stoichiometric nanowires expose local conductivity caused by crossing of the CB bottoms by Fermi levels. In the case of SrO-termination, it is prevailed upon NW facets, while in TiO_2-terminated NWs, local conductivity is more expressed around the nanowire axis. This is confirmed by analysis of projected densities of states containing mainly of O(2*p*) contributions at the top of the VB and Ti (3*d*) contribution at the bottom of the CB or around the Fermi level.

Comparison of the band edge positions and Fermi levels relatively the levels of reduction H^+/H_2 and oxidation O_2/H_2O potentials as well as analysis of the band gap widths allows us to suggest the probable STO NW configurations for application in photocatalytic splitting of water molecules under solar irradiation in the visible range. Both stoichiometric and non-stoichiometric TiO_2-terminated strontium titanate nanowires can be used as photoelectrodes, after additional structural and chemical modification of the former or directly in the latter case. On the other hand, SrO-terminated STO nanowires are rather not suitable for this purpose.

Acknowledgements

The authors acknowledge the assistance of the Saint-Petersburg State University in high-performance computations. AB and RE are grateful to Russian Foundation for Basic Research (within the Grant 14-03-00107a) while YZ is thankful to the Institute of Solid State Physics (University of Latvia, within the IMIS2 Program) for the financial support. Technical assistance of A. Chesnokov and S. Piskunov is appreciated.

Additional Supplementary Information may be found in the online version of this article.

References

[1] X. Zhu, Z. Liu, and N. Ming, *J. Nanosci. Nanotechnol*. **10**, 4109 (2010).
[2] Ph. Ghosez and J. Junquera, *First Principles Modeling of Ferroelectric Oxides Nanostructures* (In: Handbook of Theoretical and Computational Nanotechnology, Ch. **134**, Amer. Sci. Publ., Stevenson Ranch, CA, 2006).
[3] N. Nuraje and K. Su, *Nanoscale* **5**, 8752 (2013).
[4] H. Tong, S. Ouyang, Y. Bi, N. Umezawa, M. Oshikiri, and J. Ye, *Adv. Mater.* **24**, 229 (2012).
[5] H. Zhou, Y. Qu, T. Zeid, and X. Duan, *Energy Environ. Sci.*, 2012, 5, 6732
[6] J. Kang, J. Ryu, E. Ko, and Y. Tak, *J. Nanosci. Nanotechnol*. **7**, 4194 (2007).
[7] Q. Ding, Y. Yuan, X. Xiong, R. Li, H. Huang, *J. Phys. Chem. C* **112**, 18846 (2008).
[8] K. Saito and A. Kudo, *Inorg. Chem.* **49**, 2017 (2010).
[9] G.G .Yadav, G. Zhang, B. Qiu, J.A. Susoreny, X. Ruan, and Y. Wu, *Nanoscale* **3**,4078 (2011).
[10] K. Saito, K. Koga, and A. Kudo, *Dalton Trans.* **40**, 3909 (2011).
[11] T. Ma, H. Li, T. Ren, and Z. Yuan, *RSC Adv.* **2**, 2790 (2012).
[12] B. Liu, C.H. Wu, J. Miao, and P. Yang, *ACS Nano* DOI: 10.1021/nn5051954 (2014)
[13] G. Geneste, E. Bousquet, J. Junquera, and Ph. Ghosez, *Appl. Phys. Lett.* **88**, 112906 (2006).
[14] G. Pilania, S.P. Alpay, and R. Ramprasad, *Phys. Rev. B* **80**, 014113 (2009).
[15] T. Shimada, S. Tomoda, and T. Kitamura, *Phys. Rev. B* **79**, 024102 (2009).
[16] G. Pilania and R. Ramprasad, *Phys. Rev. B* **82**, 155442 (2010).
[17] G. Pilania and R. Ramprasad, *J. Mater. Sci.* **47**, 7580 (2012).

[18] Q. Fu, T. He, J.L. Li, and G.W. Yang, *J. Appl. Phys.* **111**, 124306 (2012).
[19] Q. Fu, T. He, J.L. Li, and G.W. Yang, *J. Appl. Phys.* **112**, 104322 (2012).
[20] Q. Fu, T. He, J.L. Li, and G.W. Yang, *J. Appl. Phys.* **113**, 104303 (2013).
[21] C.R.A. Catlow, Z.X. Guo, M. Miskufova, S.A. Shevlin, A.G.H. Smith, A.A, Sokol, A. Walsh, D.J. Wilson, and S.M. Woodley, *Phil. Trans. Royal Soc. A* **368**, 3379 (2010).
[22] R. Memming, *Semiconductor Electrochemistry* (Wiley-VCH Verlag, Germany, 2001).
[23] S. Chen and L.W. Wang, *Chem. Mater.* **24**, 3659 (2012).
[24] A. Kudo and Y. Miseki, *Chem. Soc. Rev.* **38**, 253 (2009).
[25] M.F.C. Gurgel, J.W.M. Espinosa, A.B. Campos, I.L.V. Rosa, M.R. Joyad, A.G. Souzab, M.A. Zaghete, P.S. Pizani, E.R. Leite, J.A. Varela, and E. Longo, *J. Luminesc.* **126**, 771 (2007).
[26] Y. Xu and M.A. Schoonen, M. A. *Amer. Mineralogist* **85**, 543 (2000).
[27] M.S. Wrighton, D.L. Morse, A.B. Ellis, D.S. Ginley, and H.B. Abrahamson, *J. Amer. Chem. Soc.* **98**, 2774 (1976).
[28] S. Hara and H. Irie, *Appl. Catal. B* **115-116**, 330 (2012).
[29] R. Konta, T. Ishii, H. Kato, and A. Kudo, *J. Phys. Chem. B* **108**, 8992 (2004).
[30] T. Puangpetch, T. Sreethawong, and S. Chavadej, *Intern. J. Hydrog. Energy* **35** 6531 (2010).
[31] K. Iwashina and A. Kudo, *J. Amer. Chem. Soc.* **133**, 13272 (2011).
[32] S. Ouyang, H. Tong, N. Umezawa, J. Cao, P. Li, Y. Bi, Y. Zhang, and J. Ye, *J. Amer. Chem. Soc.* **134**, 1974 (2011).
[33] J. Liu, Y. Sun, Z. Li, S. Li, and J. Zhao, *Intern. J. Hydrog. Energy* **36**, 5811 (2011).
[34] H. Bai, J. Juay, Z. Liu, X. Song, S.S. Lee, and D.D. Sun, *Appl. Catal. B* **125**, 367 (2012).
[35] R. Dovesi, V.R. Saunders, C. Roetti, R. Orlando, C. M. Zicovich-Wilson, F. Pascale, B. Civalleri, K. Doll, N.M. Harrison, I.J. Bush, Ph. D'Arco, M. Llunell, M. Causá, and Y. Noël, *CRYSTAL14 User's Manual* (University of Turin, Turin, 2013).
[36] J.P. Perdew, M. Ernzerhof, and K. Burke, *J. Chem. Phys.* **105** 9982 (1996).
[37] C. Adamo and V. Barone, *J. Chem. Phys.* **110**, 6158 (1999).
[38] A. Schäfer, C. Huber, and R. Ahlrichs, *J. Chem. Phys.* **100**, 5829 (1994).
[39] L.A. LaJohn, P.A. Christiansen, R.B. Ross, T. Atashroo, and W.C. Ermler, *J. Chem. Phys.* **87**, 2812 (1987).
[40] M.M. Hurley, L.F. Pacios, P.A. Christiansen, R.B. Ross, and W.C. Ermler, *J. Chem. Phys.* **84**, 6840 (1986).
[41] R.A. Evarestov, E. Blokhin, D. Gryaznov, E.A. Kotomin, and J. Maier, *Phys. Rev. B* **83**, 134108 (2011).
[42] R.A. Evarestov, A.I. Panin, A.V. Bandura, and M.V. Losev, *J. Phys.: Conf. Ser.* **117**, 012015 (2008).
[43] W.H. Press, S.A. Teukolski, V.T. Vetterling, and B.P. Flannery, *Numerical Recipes in FORTRAN 77: The Art of Scientific Computing* (University of Cambridge, New York, 2001).
[44] H.J. Monkhorst and J.D. Pack, *Phys. Rev. B* **13**, 5188 (1976).
[45] B. Meyer, J. Padilla, and D. Vanderbilt, *Faraday Discuss.* **114**, 395 (1999).
[46] K. Reuter, C. Stampfl, M. Scheffler, Chapter 1 in: *Handbook of Materials Modeling* (Ed. S. Yip, Springer Verlag, Netherlands, 2005), pp 149-194.
[47] M.W Chase, *JANAF Thermochemical Tables* (4rd Ed.), In: *J. Phys. Chem. Ref. Data*, Monograph 9 (1998).
[48] F. Pascale, C.M. Zicovich-Wilson, F. Lopez, B. Civalleri, R. Orlando, and R. Dovesi, *J. Comput. Chem*. **25**, 888 (2004).
[49] E. Heifets, S. Piskunov, E.A. Kotomin, Yu.F. Zhukovskii, and D.E. Ellis, *Phys. Rev. B* **75**, 115417 (2007).
[50] R.A. Evarestov and Yu.F. Zhukovskii, *Surf. Sci.* **608**, 226 (2013).
[51] Yu.F. Zhukovskii, S. Piskunov, J. Begens, J. Kazerovskis, and O. Lisovski, *phys. status solidi (b)* 250, **793** (2013)